İSTANBUL UNIVERSITY
C E R R A H P A Ş A

Design and Analysis of Time-Varying Derivative Fractional Order Proportional–Integral–Derivative Controller for Frequency Regulation of Shipboard Microgrid System

Sonalika Mishra[ID]**, Pratap Chandra Nayak**[ID]**, Ramesh Chandra Prusty**[ID]**, Sidhartha Panda**[ID]

Department of Electrical Engineering, Veer Surendra Sai University of Technology, Odisha, India

ABSTRACT

This study considers the shipboard microgrid (MG) system's frequency oscillations problem against the unpredictability of renewable resources and load uncertainties. The shipboard MG system consists of a photovoltaic, wind turbine generator, ship diesel generator, electrolyzer-based fuel cells, and battery energy storage system. A time-varying derivative fractional order controller (TVD-FOPID) has been incorporated into the shipboard MG system to attain the desired frequency stability. In this respect, the introduction of the time function to the derivative part of the TVD-FOPID controller provides appropriate damping at the proper instant to reduce the voltage spike sufficiently which improves the system response. Consequently, a modified sine cosine algorithm (MSCA) has been employed for the tuning of the TVD-FOPID controller's coefficient. There is a 13.43% improvement in fitness value with MSCA against the basic SCA-tuned TVD-FOPID controller with diversified unpredictable disturbances. About, 80% reduction is observed in the derivative kick and a 40% reduction is observed in the voltage spike with the use of a tuned TVD-FOPID controller over MSCA-tuned TV-FOPID. Again, 86% reduction in a derivative kick and, a 99% reduction in voltage spike with the use of a TVD-FOPID controller than that of a regular FO-PID controller. The simulation results validate that the TVD-FOPID controller offers stable output in less time than TV-FOPID and FOPID controllers. Also, it is confirmed that the derivative kick, voltage spikes, and the peak overshoot of the response offered by the proposed approach are decreased, which will save the system components. Further, the viability of the controller has been evaluated through sensitivity analysis. To witness the real-time application of the simulated system results are examined in the OPAL-RT simulator.

Index Terms—Shipboard microgrid, modified sine cosine algorithm (MSCA), load frequency control, fractional order PID control, time-varying fractional order PID control

NOMENCLATURE

PID	Proportional–integral–derivative	MG	Microgrid
TV-FOPID	Time-varying fractional order proportional–integral–derivative controller	TVD-FOPID	Time-varying derivative fractional order proportional–integral–derivative controller
MSCA	Modified sine cosine algorithm	PV	Photovoltaic
WT	Wind turbine	FC	Fuel cell
AE	Aqua electrolyzer	DG	Diesel generator
RES	Renewable energy system	SWE	Sea wave energy
BESS	Battery energy storage system	LFC	Load frequency control
MVO	Multi-verse optimizer	V2G	Vehicle 2 Grid
P+ID	Proportional plus integral–derivative	AGC	Automatic generation control
FOPI-FOPTID	Fractional order proportional integral–fractional order proportional tilt integral derivative	G_{WTG}	Transfer function of wind turbine generator

K_{WTG}	Gain of wind turbine generator		T_{WTG}	Time constant of the WT system
G_{PV}	Gain of photovoltaic system		K_{PV}	Gain of photovoltaic system
T_{PV}	Time constant of photovoltaic system		G_G	Gain of governor
G_T	Gain of turbine		G_{FC}	Gain of fuel cell
T_{FC}	Time constant of fuel cell		G_{AE}	Gain of aqua electrolyzer
T_{AE}	Time constant of aqua electrolyzer		G_{INV}	Gain of inverter
T_{INV}	Time constant of inverter		G_{FIT}	Gain of filter
T_{FIT}	Time constant of filter		G_{BESS}	Gain of battery energy storage system
K_{BESS}	Gain of battery energy storage system		T_{BESS}	Time constant of battery energy storage system
M	Inertia constant		D	Damping constant
P_s	Source power		P_L	Load power
ΔP_e	Net power deviation		Δf	Frequency Deviation
K_{SYS}	Gian of power system		G_{SYS}	Transfer function of power system
${_a D_t^\alpha f(t)}$	Non-integer fundamental operator		α	Real order of the differintegral
K_P	Proportional gain		K_I	Integral gain
K_D	Derivative gain		λ	Fractional integral order
μ	Fractional derivative order		$K_P(t)$	Time-varying proportional gain
$K_I(t)$	Time-varying integral gain		$K_D(t)$	Time-varying derivative gain
α_P	Time constant parameter of proportional controller		α_I	Time constant parameter of integral action
α_D	Time constant parameter of derivative action			

I. INTRODUCTION

Maritime transport plays a crucial role in international trade, as it participates in almost three-quarters of global transportation. It is the most efficient way of energy transportation in the form of cargo. It is associated with about 2% of energy related to CO_2 emissions. Urge to the climate targets of the Paris Agreement, the IMO has a target to reduce CO_2 emissions by 50% before the year 2050. Electrification of transportation channels is now straightforward to the environmental policy objectives. Interpretation of renewable energy sources and energy-storing elements is now mostly welcomed by researchers in electrical background [1]. A ship power vessel clustered with photovoltaic (PV), wind turbine generator (WT), diesel generator (DG), fuel cell (FC), and energy-storing elements can be considered an islanded microgrid (MG). A variety of research has been done utilizing islanded MG in maritime vessels in [2–5]. The stability analysis of a ship power vessel consisting of renewable energy sources (RES) with energy storage is analyzed in [2]. A combination of diesel/solar and battery systems is utilized as a power system in a ship environment maritime crane operation is well discussed in[3]. An islanding MG clustering PV/wind/fuel cell/battery system is employed in ship power vessels and its delay-dependent stability analysis was done in [4]. In [5], a mobile islanded microgrid comprising of PV/wind/sea wave energy (SWE) and battery energy storage system is used as a marine vessel power system.

The environmental policy for the reduction of CO_2 emission for electricity generation in transportation systems targets the use of RES and energy storage systems (ESS) [5]. Many researchers have performed intensive analysis in shipboard MG systems to establish frequency stability. For solving load frequency control (LFC) issues, the design of PID controller with linear quadratic Gaussian method is well addressed in [6]. Multi-verse optimizer (MVO) technique [7] and the advancement of the search process of the salp swarm algorithm [8] for global optimization problems are used for solving the LFC issues of microgrid systems. The LFC study of an islanded microgrid system is evaluated with the presence of vehicle-to-grid (V2G) technology [9] using a fuzzy type II P+ID controller [10]. JAYA algorithm optimized integral double derivative controller for LFC of a PV-thermal based power system is explored in [11]. Automatic generation control (AGC) of a multi area multisource power system comprising wind, hydro, thermal and gas generation units is addressed in [12]. Worth utilization of network resources for LFC design of an isolated power system is well discussed in [13, 14]. Cascade FOPI-FOPTID controller with energy storage devices for AGC performance advancement of electric power systems is demonstrated in [15]. A novel load frequency control scheme for an interconnected two-area power system including wind turbine generation and redox flow battery is established in [16]. Hybrid whale optimization algorithm with simulated annealing based fractional-order type 2 Fuzzy PID controller used for improved frequency regulation of hybrid system [17]. The contribution of gate-controlled series capacitor

to regulate the frequency in multi-area power systems considering time delays is shown in [18]. The frequency stability of an islanded microgrid using a novel virtual inertia control and a fractional order cascade controller is stated in [19]. An improved equilibrium optimization-based fuzzy tilted double integral derivative with a filter controller [20] is implemented in the MG system for the betterment of frequency stability. A sine cosine-based fractional order proportional–integral–derivative controller (FOPID) controller is successfully implemented for the LFC study of the hybrid power system [21, 22]. The fruitful execution of the sine cosine algorithm is well discussed in [23–25]. Type II fuzzy PI controller is well addressed for solving LFC issues in [26]. The variable wind turbine design is well addressed for reducing the inertia of the grid [27]. Load frequency control of a wind-PV with energy storage system-based hybrid power system is analyzed in [28]. Type 2 fuzzy systems with PI controllers are implemented in [29]. Two-degree-of-freedom PID controllers are successfully demonstrated for load frequency control application in [30]. For the LFC study of a multi-microgrid system, an integral tilt derivative with filter controller controller is implemented in [31]. To mitigate derivative kick by fractional order PID controller is described in [32]. The tolerance of FOPID controller due to time delay is analyzed using Bode's transfer function model to evaluate the robustness of a nonlinear system [33]. The butterfly optimization algorithm (BOA) scaled FOPID-based frequency control strategy has been proposed to reduce the frequency oscillations with highly fluctuating propulsion load and RESs in shipboard MG system [34]. To establish improved frequency stability, the chaotic BOA-based cascaded PI-TID controller is proposed in hybrid MG system [35]. The disruption of shipboard MG's frequency due changes in the weather conditions or loads has been stabilized by direct search algorithm based fractional-order system [36]. The time delay analysis of type II fuzzy fractional order controller for LFC of modern marine power grids has been studied using stability boundary locus method [37]. However, the researchers are not giving so much attention to the control of voltage spikes called derivative kicks in microgrid systems for solving LFC issues. So, the main contribution of the research work is as follows:

1. A shipboard MG is modeled to establish improved frequency stability using MSCA based time-varying derivative (TVD)-FOPID approach against the nonlinear performance of WT, PV, DG, FC, AE, and BESS.
2. A TVD-FOPID controller is designed and established as a secondary load frequency controller of the shipboard MG system.
3. The novel approach of the modified sine cosine algorithm (MSCA) is executed for fine-tuning the considered TVD-FOPID controller.
4. The performance of the maiden TVD-FOPID controller is compared with TV-FOPID and existing FOPID controllers under various disturbances of solar energy, wind energy, step load perturbation, and random load perturbation.
5. The sensitivity analysis and the robustness of the proposed controller are tested under varied parameters of the system.
6. The practicality of the proposed system has been validated through OPAL-RT setup, and the proposed method outcomes are mapped with recent research methods to present the efficacy of the method.

The remaining part of the paper is organized as follows: The component of the shipboard MG system and their transfer function modeling is described in Section II. The FOPID, TV-FOPID, and TVD-FOPID control structure is presented in Section III. The modified sine cosine algorithm is presented in Section IV. Section V represents the simulation result analysis of 3 different case studies of the proposed shipboard microgrid system under the simultaneous disturbance of wind, solar, and multi-step load perturbation. The conclusion part is addressed in Section VI.

II. SYSTEM UNDER STUDY

A 0.5 MW rated shipboard MG system has been considered for this study as illustrated in Fig. 1, which includes WT, DG, FC, and BESS. Here the PV and WTG sources are used to maintain the load demand of the ship MG system. The ratings of PV and WTG plants are 60 KW and 120 KW respectively. The surplus power produced from PV/WTG sources is stored as hydrogen for FC with the support of ES. When there is a chance of a decrease in power production, the energy supply is maintained with the help of FC. The rating of the fuel cell unit used in this system is 70 KW. A DG system of 200 KW is considered for this study as a back-of generator in a situation where the RES system does not sufficiently meet the load demand of a shipboard MG system. Again, a BESS of 50 KW is considered for this study to manage critical loading conditions in the shipboard MG system. The transfer function modeling ship MG system is illustrated in Fig. 2.

To simulate the shipboard MG system, the modeling of WT, PV, DG, FC, and AE are analyzed with their dynamic higher order nonlinear equations. However, for small signal LFC studies of shipboard MG systems, the transfer function models are preferred. So, individual components of the ship MG system are represented by their transfer functions.

A. Modeling of Wind Turbine System
The wind turbine model is represented by Eq. (1) referred from [4] as:

$$G_{WTG} = \frac{K_{WTG}}{1 + sT_{WTG}} \tag{1}$$

where K_{WTG} and T_{WTG} are the gain and time constant of the WT system. The values of K_{WTG} and T_{WTG} are equal to 1,1.5 respectively.
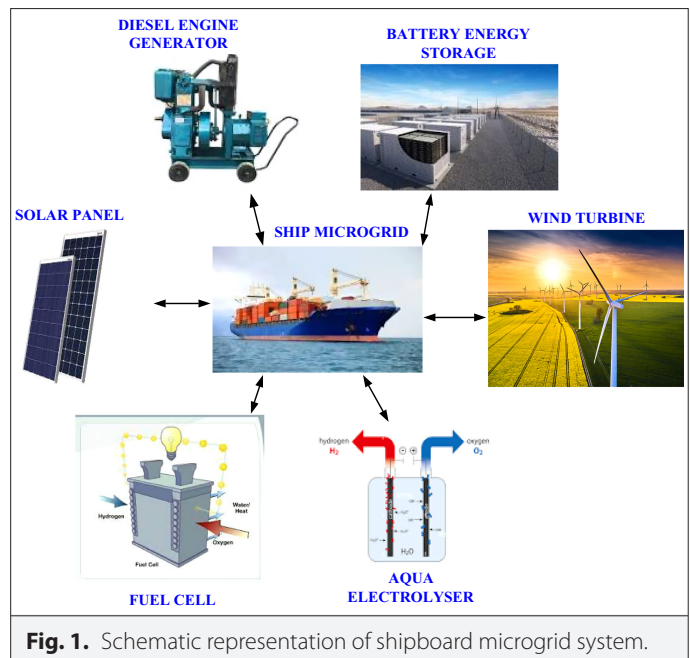

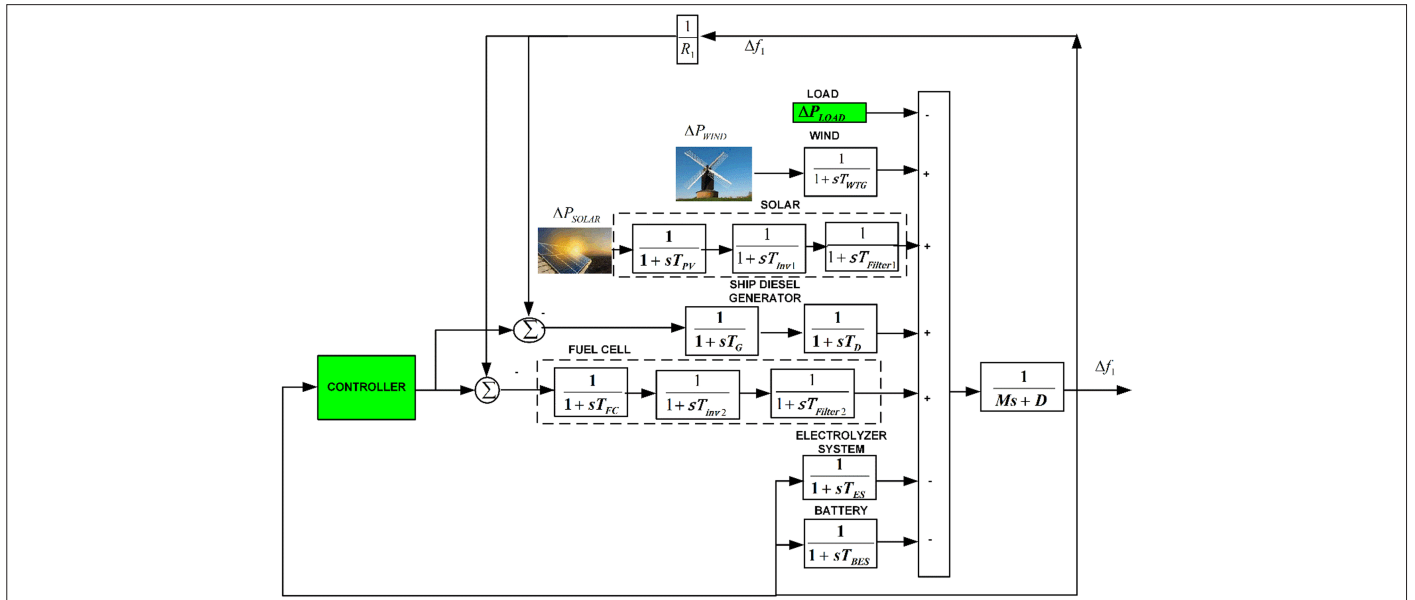**Fig. 1.** Schematic representation of shipboard microgrid system.

Fig. 2. Topology of ship microgrid with a secondary controller.

B. Modeling of PV System

The PV model is represented by Eq. (2) referred to [5] as:

$$G_{PV} = \frac{K_{PV}}{1+sT_{PV}} \tag{2}$$

where K_{PV} and T_{PV} are the gain and time constant of the System. The values of K_{PV} and T_{PV} are equal to 1, and 1.5 respectively.

C. Modeling of Diesel Generator

A DG unit in the ship MG system is used as a back of propose in a situation where PV and WT systems are unable to meet the demand of the ship MG system. The ship DG contains two simplified blocks of governor is provided by Eq. (3) referred from [7] and the generator is given by Eq. (4) referred from [7].

$$G_G = \frac{1}{1+sT_G} \tag{3}$$

$$G_T = \frac{1}{1+sT_D} \tag{4}$$

The gain of the governor and generator is equal to 1 and its time constant T_G and T_D is equal to 0.08 and 0.4.

D. Modeling Fuel Cell Unit

The FC model is represented by Eq. (5) referred to [9] as:

$$G_{FC} = \frac{1}{1+sT_{FC}} \tag{5}$$

where the gain of the FC is equal to 1 and the time constant T_{FC} is equal to 0.26.

E. Modeling of Aqua Electrolyzer

The AE model is represented by Eq. (6) referred to [9] as:

$$G_{AE} = \frac{1}{1+sT_{AE}} \tag{6}$$

Where the gain of the AE is equal to 1 and the time constant T_{AE} is equal to 0.26.

F. Modeling of Inverter

The inverter model is represented by Eq. (7) referred to [5] as

$$G_{INV} = \frac{1}{1+sT_{INV}} \tag{7}$$

where the gain of the inverter is equal to1 and the time constant T_{INV} is equal to 0.4

G. Modeling of Filter

Modeling of the filter is presented by Eq. (8) referred from [9] as:

$$G_{FIT} = \frac{1}{1+sT_{IFIT}} \tag{8}$$

Where the gain of the filter is equal to 1, and the time constant T_{FIT} is equal to 0.004.

H. Modeling of Energy Storing Element

Modeling of energy storing elements by Eq. (9) referred from [17] as

$$G_{BESS} = \frac{K_{BESS}}{1+ST_{BESS}} \tag{9}$$

where K_{BESS} the gain of the filter is equal to 1, and time constant T_{BESS} is equal to 0.01.

I. Power and Frequency Deviation

For stable operation of the ship MG system, the power generated from PV and WT are effectively controlled to meet the demand of the

ship MG system. So, power control approaches are extensively used. This control approach is based on source power (P_s) and load power (P_L) is shown in Eq. (10) [22]. The load frequency deviation is dependent on the net power deviation as shown in Eq. (11) [22]. K_{SYS} is the frequency characteristic constant presented in Eq (12) [22].

$$\Delta P_e = P_S - P_L \tag{10}$$

$$\Delta f = \frac{\Delta P_e}{K_{SYS} + D} \tag{11}$$

$$G_{SYS} = \frac{\Delta f}{\Delta P_e} = \frac{1}{Ms + D} \tag{12}$$

Here M, D is termed as inertia constant and damping constant. The values M and D are 0.2, 0.12 respectively in the model under study the regulation constant 'R' is 3.

III. FRACTIONAL ORDER PROPORTIONAL–INTEGRAL–DERIVATIVE CONTROLLER

The design of the FOPID controller is based on fractional calculus which brings the non-integer integral and differential order to the conventional PID controller. The non-integer fundamental operator is $a^{D_t^{\alpha f(t)}}$ is presented by Eq. (13) [7].

The value of

$$a^{D_t^{\alpha f(t)}} = \frac{d^\alpha f(t)}{\left[d(t-a)\right]^\alpha} \tag{13}$$

Here, "a" and "t" are the limits of operation, "α" signifies the real order of the differ-integral and $\alpha \in R$, since "a" represents the lower limit, it is considered to be zero if not expressed.

The Laplace transform of Eq. (13) is presented by Eq. (14).

$$LD^{\pm\alpha}f(t) = s^{\pm\alpha}.F(s). \tag{14}$$

The FOPID controller structure is demonstrated in Fig. 3. In the Laplace domain, the general equation of this controller is presented by Eq. (15),

$$P(s) = \frac{U(s)}{E(s)} = K_P + \frac{K_I}{s^\lambda} + K_D.s^\mu, \text{here}\lambda, \mu \in \left[0,1\right] \tag{15}$$
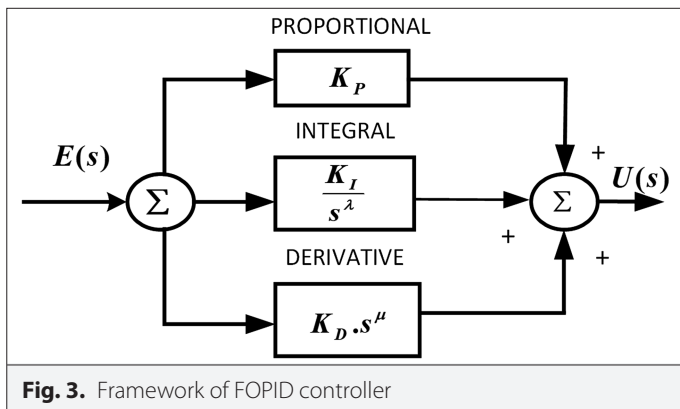
λ and μ are the fractional order of integrator and differentiator. Kp, K_I, K_D are the proportional, integral and derivative constants. The value of λ and μ decides the function of the PID/PD/PI in the FOPID structure, the value of λ, μ can be any non-integer number between 0 and 1. Thus, for the FOPID controller the operating range and stability region for controller action increases. Hence it improves the steady-state response and overall dynamics of a closed-loop system. For any sudden change of input signal, the derivative controller gives a huge spike in its control signals called derivative kick. These spikes in the control signal can harm the control system and system services. So, while designing a controller the reduction of the derivative kick should be investigated. In this research work time varying FOPID controllers are proposed. This controller does its control action depending upon a time function.

A. Structure of Time-Varying Fractional Order PID Controller
In this section, the TV-FOPID structure as presented in Fig. 4 has been discussed. The basic parameters of this controller structure are $K_P(t)$, $K_I(t)$, $K_D(t)$, λ, μ. These are expressed by Eqs. (16–18) [32].

$$K_P(t) = K_P\left(1 - e^{-\alpha_p t}\right), t \geq 0 \tag{16}$$

$$K_I(t) = K_I\left(1 - e^{-\alpha_I t}\right), t \geq 0 \tag{17}$$

$$K_D(t) = K_d\left(1 - e^{-\alpha_d t}\right), t \geq 0 \tag{18}$$

Here K_p, K_I, K_d are the gain parameters and α_p, α_I, and α_D are the time constants parameters for fractional proportional, integral, and derivative control action respectively.

B. Time-Varying Derivative FOPID Controller Structure
In this section, the proposed TVD-FOPID structure is presented in Fig. 5 [32]. Unlike the TV-FOPID controller, only the derivative controller action is made time-varying and the rest of the controller action (proportional/integral) are left time-invariant as in the basic FOPID controller structure. Thus, the parameters of the proposed time-varying derivative controller are K_P, K_I, $K_D(t)$, λ, and μ. This controller does its control action by providing its derivative action gradually. For the earlier duration, it nullifies its derivation control action, but at the later duration, it allows it to participate in the control action.

It can be analyzed from Figs. 4 and 5. An optimal time function is multiplied by the derivative action of the controller. The $K_D(t)$ is the time-varying variable.
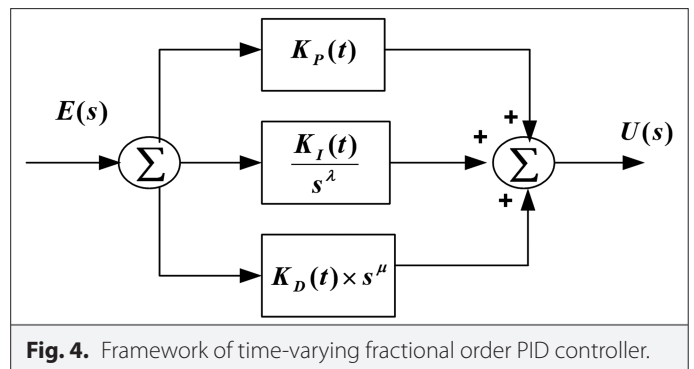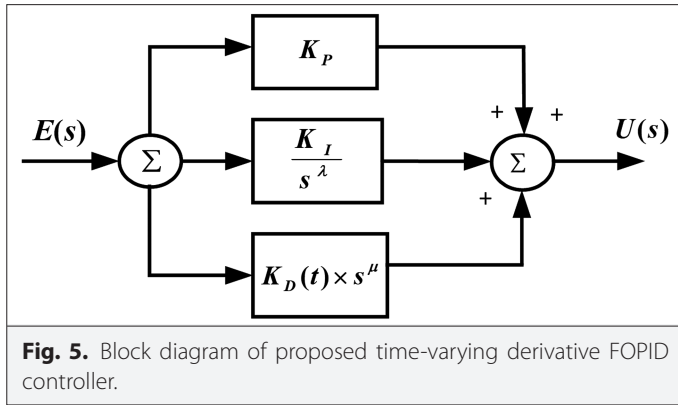

Fig. 3. Framework of FOPID controller

Fig. 4. Framework of time-varying fractional order PID controller.

Fig. 5. Block diagram of proposed time-varying derivative FOPID controller.

IV. MODIFIED SINE COSINE ALGORITHM

This stochastic algorithm is based on sine cosine mathematical functions [22–25]. It starts execution with a randomly chosen candidate solution. The solutions are improved by migration towards or outward from the target position. This algorithm also suffers from the imperfect balance of exploration and exploitation. For this reason, it exhibits premature convergence. To eradicate the drawbacks of SCA, the MSCA [22] focuses on the proper balance of exploration and exploitation. In SCA the balance between these two phases of optimization is achieved by the random number r_1 is expressed by Eq. (25) as:

$$r_1 = a - t \frac{a}{T_{max}} \qquad (19)$$

The larger value of r_1 is responsible for better global searching and the lower value of r_1 is responsible for better local searching of the algorithm. So, the value of r_1 is made to decrease from the beginning of the iteration to the maximum iteration set by the user. For updating the value of r1 different methods such as the linear decreasing method, exponential decreasing method, and parabola decreasing method are described in [25]. In this case, it is proved that the exponential decreasing method for r_1 is better in contrast to the other two decreasing methods. Again, a maiden attempt is considered for modification of the exponential decreasing method. This modification is represented by Eq. 20 [25] as:

$$r_1 = a - t^c \frac{a}{T_{max}^c} \qquad (20)$$

Where "a" is a fixed constant. The original value of "a" is 2. The values of "a" and "c" are tested over a range of 0-∞, while keeping one variable fixed. After observing the results, the best value of "a" and "c" obtained are 1.5 and 1, respectively. The detailed analysis of the MSCA algorithm can be better understood from [22].

To test the supremacy of the proposed MSCA algorithm, this algorithm is tested for 5 benchmark functions and its comparison with other existing metaheuristic techniques in terms of average (avg) and standard deviation (SD) values are shown in Table I. The details of the unimodal test function considered are shown in Table I.

The experimental verification of the MSCA algorithm shown in Table I concludes that the MSCA algorithm offers the best values as compared to other conventional algorithms. The best values obtained are highlighted in bold. Only for function "Rosenbrock" the best

average value is offered by the SCA algorithm. After verification of the competence of the MSCA algorithm, this algorithm is utilized to design a secondary load frequency controller for the ship microgrid system. The flowchart of the MSCA has been presented in Fig. 6.

It is important to define the objective function to run an optimization algorithm to solve any major task. The objective function defined for this study is the integral square error (ISE), which can be expressed by Eq. 21 [20]:

$$ISE = \int_0^{t_{sim}} \left| \left(\Delta f + \Delta u \right)^2 \right| dt \qquad (21)$$

V. RESULT AND DISCUSSION

In this section, the accuracy of the suggested controller approach for the shipboard MG System is examined under different case studies. In case 1, the efficacy of the MSCA technique-based TVD-FOPID controller is tested under the simultaneous disturbance of wind, solar, and multi-step load perturbation conditions. In case 2, a comparative analysis is carried out for the TVD-FOPID/TV-FOPID/FOPID controller with the MSCA technique under the same scenario as case 1. To examine the robustness of the proposed MSCA-based TVD-FOPID controller the nominal parameters of the microgrid system are varied in the −15% to +45% range in case 3. In case 4, the sturdiness of the TVD-FOPID controller is tested under random load variation with the variation of wind and solar power. In case 5, the validation of OPAL-RT is provided for the practical feasibility of the proposed approach. Last, the proposed result outcomes are compared with recent research scenarios in case 6.

A. Case 1: Technique Comparison
The efficacy of the suggested method is carefully investigated by considering its performance under the simultaneous disturbance of wind, solar and multi-step load perturbation. The considered wind input data for wind turbine, solar power variation, and multi-step load is injected into the system as shown in Fig. 7a–c. The output frequency curve and controller output curve are shown in Figs. 8 and 9. From Figs. 8 and 9, it is noticed that the MSCA-based TVD-FOPID controller is offering stable output in less time as compared to SCA tuned TVD-FOPID controller. The gain parameter and error value obtained from MSCA/SCA-tuned TVD-FOPID parameters are recorded in Table II. It is noticed that MSCA-based ISE-0.038 and SCA-based ISE-0.44. This indicates error value (ISE) is decreased by 13.63% as compared to SCA tuned TVD-FOPID controller.

B. Case 2: Controller Comparison
Furthermore, with the MSCA technique the supremacy of TVD-FOPID is compared with TV-FOPID and FO-PID controllers. The gain parameter obtained from MSCA tuned TVD-FOPID/TV-FOPID/FOPID controller's parameters are presented in Table III. Fig. 10 represents frequency deviations and the transient parameters such as overshoot (OS), undershoot (US) and settling time (TS) are recorded in Table IV. It is clearly noticed that The ISE (0.038) is less related to TV-FOPID and FOPID controller. The TVD-FOPID (OS = 0.1294, US = 0.2252 and TS = 0.0041), The TV FOPID (OS = 1.0079, US = 0.3979 and TS = 0.0025) and FOPID (OS = 1.8148, US = 1.8052 and TS = 1.3264). Fig. 11 represents the output voltage offered by the FOPID/TV-FOPID/TVD-FOPID controller. It is observed that the voltage spike produced by regular FOPID controller is (4.7 P.U.), TV-FOPID is (3 P.U.) and proposed TVD-FOPID is (0.005 P.U.) about, 40% of reduction is observed in the

TABLE I. COMPETENCE OF MSCA ALGORITHM WITH EXISTING TECHNIQUES ON UNIMODAL TEST FUNCTIONS

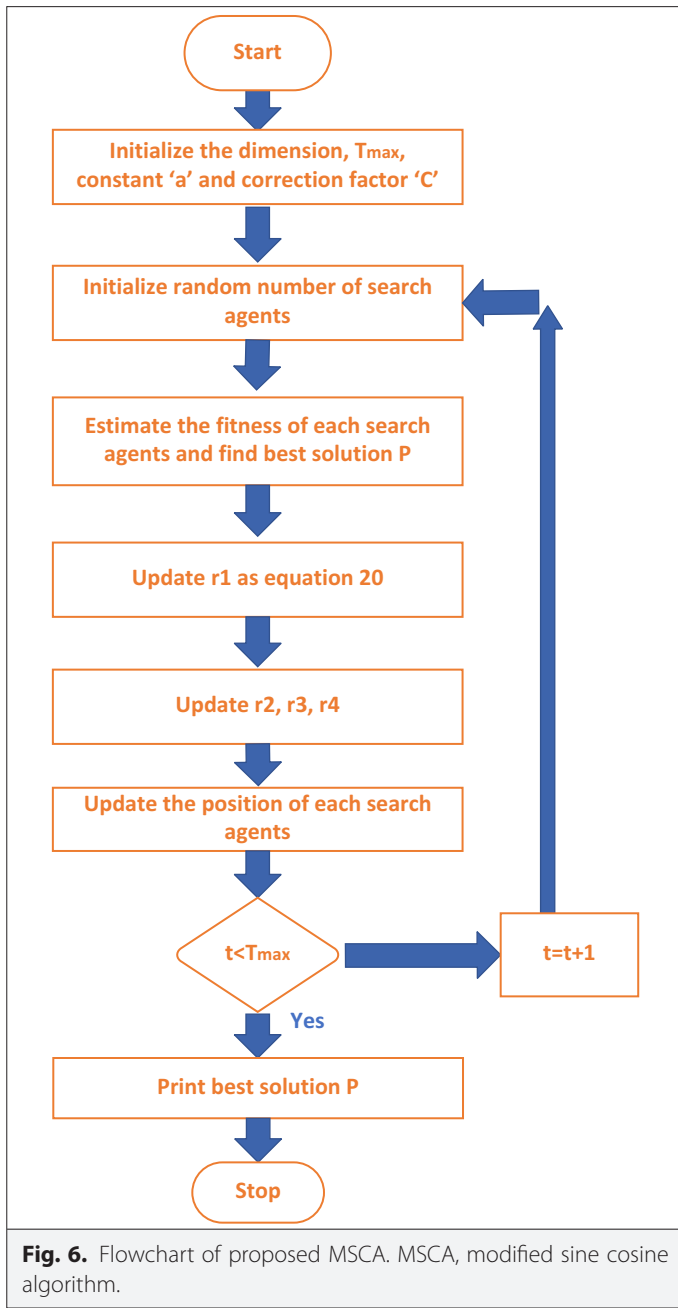| Function Name	Test Function	Range	Algorithm	Avg	SD
Sphere	$F_1(x) = \sum_{i=1}^{n} x_i^2$	[−100,100]	MSCA	**1.23E-105**	**6.90E-105**
			SCA	**6.36E-22**	3.82E-21
			MVO	2.249	1.499
			GWO (Grey Wolf Optimizer)	2319.10	1237.10
			GSA (Gravitational Search Algorithm)	2983.66	903.38
			PSO (Particle Swarm Optimization)	3.552	2.8537
			GA (Genetic Algorithm)	27 187.58	2745.82
Schwefel	$F_2(x) = \sum_{i=1}^{n} |x_i| + \prod_{i=1}^{n} |x_i|$	[−10,10]	MSCA	8.97E-63	2.14E-62
			SCA	1.76E-16	1.17E-15
			MVO	15.92	44.7559
			GWO	14.431	5.92
			GSA	10.9651	10.549
			PSO	**8.716**	**4.929**
			GA	68.661	6.0623
Rastrigin	$F_3(x) = \sum_{i=1}^{n} (\sum_{j-1}^{i} x_j)^2$	[−100,100]	MSCA	**7.66E-58**	**2.99E-05**
			SCA	1.39E-05	8.71E-05
			MVO	453.200	177.097
			GWO	7278.133	2143.11
			GSA	113,740.4	78 786.75
			PSO	2380.96	1183.35
			GA	48 530.01	8249.75
Ackley	$F_4(x) = \max_i \{|x_i|, 1 \leq i \leq n\}$	[−100,100]	MSCA	**2.65E-39**	**7.94E-39**
			SCA	3.27E-07	6.29E-07
			MVO	38.33	13.94
			GWO	13.097	11.346
			GSA	32.256	6.227
			PSO	21.5169	6.716
			GA	62.993	2.535
Rosenbrock	$F_5(x) = \sum_{i=1}^{n-1} \left[100(x_{i+1} - x_i^2)^2 + (x_i - 1)^2 \right]$	[−30,30]	MSCA	**5.7736**	3.559E-01
			SCA	7.113	**0.41179**
			MVO	1024.13	1309.434
			GWO	3,425,462	3 304,309
			GSA	7582.498	7314.818
			PSO	1132.456	1357.967
			GA	65 361,620	29 714,021

MSCA, modified sine cosine algorithm; MVO, multi-verse optimizer; SCA, sine cosine algorithm; GA, Genetic Algorithm; PSO, Particle Swarm Optimization; GSA, Gravitational Search Algorithm; GWO, Grey Wolf Optimizer.

voltage spike with the use of TV-FOPID controller again 99% reduction in voltage spike to regular FO-PID controller. It is indicated that the derivative kick is reduced with the use of the TVD-FOPID controller. It concludes that the TVD-FOPID controller offers stable output in less time as compared to TV-FOPID and FOPID controllers, which will save the life of the batteries and other control system apparatuses. The stability of the system controlled by the proposed TVD-FOPID controller is evaluated with frequency response analysis. The frequency stability of the shipboard MG system is shown in Fig. 12 indicating the gain margin is infinite and the phase margin is 90.6 degrees.

C. Case 3: Sensitivity Analysis of the Proposed Controller
To explore the robustness of the proposed controller the parameters of the ship microgrid are varied by some ranges as shown in Table V. The optimal controller parameters used in the previous scenario are kept constant. The output frequency curve offered by the proposed TVD-FOPID controller is contrasted with TV-FOPID and FOPID controllers as shown in Fig. 13. It is concluded that the offered frequency

is improved by the proposed method. The mitigation of derivative kick is also maintained as in the previous case in sight of the changed parameters. The controller output voltage signal is depicted in Fig. 14. About 5 P.U. voltage spikes in a cyclic manner are outputted by the FOPID controller. with the introduction of the TV-FOPID controller, the voltage spike is reduced to approx. 3 P.U. for a smaller period of time. The reduction in voltage spike achieved is about 40%. The control action of the TVD-FOPID controller has shown supremacy over other control actions by reducing the voltage spikes by 99%. The voltage spike offered by this control action is 0.002P.U. which lasts for a few microseconds. As shown in Fig. 14. The value of OS, US, TS and fitness value LFC for this scenario is tabulated in Table VI. This confirms that the proposed controller is giving minimum values for all the overshoot, undershoot, and settling time and ISE values than other participant controllers. This investigation entails that the peak values are achieved in less time with the employment of the TVD-FOPID controller. There are no significant changes observed in the transient values that were outputted in the previous case. The superlative control action of the proposed TVD-FOPID controller is

Fig. 6. Flowchart of proposed MSCA. MSCA, modified sine cosine algorithm.

Fig. 7. (a) Fluctuating solar power generation, (b) Fluctuating wind power generation, (c) Fluctuating power demand.

evaluated in terms of the smooth operation of $\triangle P_{BESS}$, $\triangle P_{FC}$, $\triangle P_{DEG}$, $\triangle P_{PV}$ and $\triangle P_{WIND}$ as shown in Figs. 15-19 which conclude the superlative performance of the proposed TVD-FOPID controller as compared to other participating controllers.

D. Case 4: Performance Analysis of the Proposed Controller With Random Load, Solar and Wind Source Deviation
To make a realistic analysis a random load pattern is considered shown in Fig. 20. Here the random load is injected into the simulated system along with the solar and wind deviation as shown in Figs. 18 and 19, respectively. The output response FOPID, TV-FOPID and the proposed TVD-FOPID of the ship MG system are analyzed. It is confirmed from the output responses given in Figs. 21 and 22, that the proposed controller is offering better output frequency as

Fig. 8. Controller output signal for technique comparison.
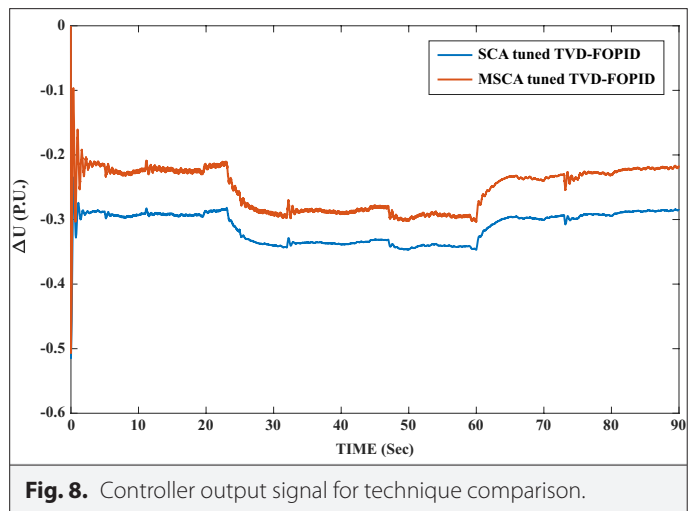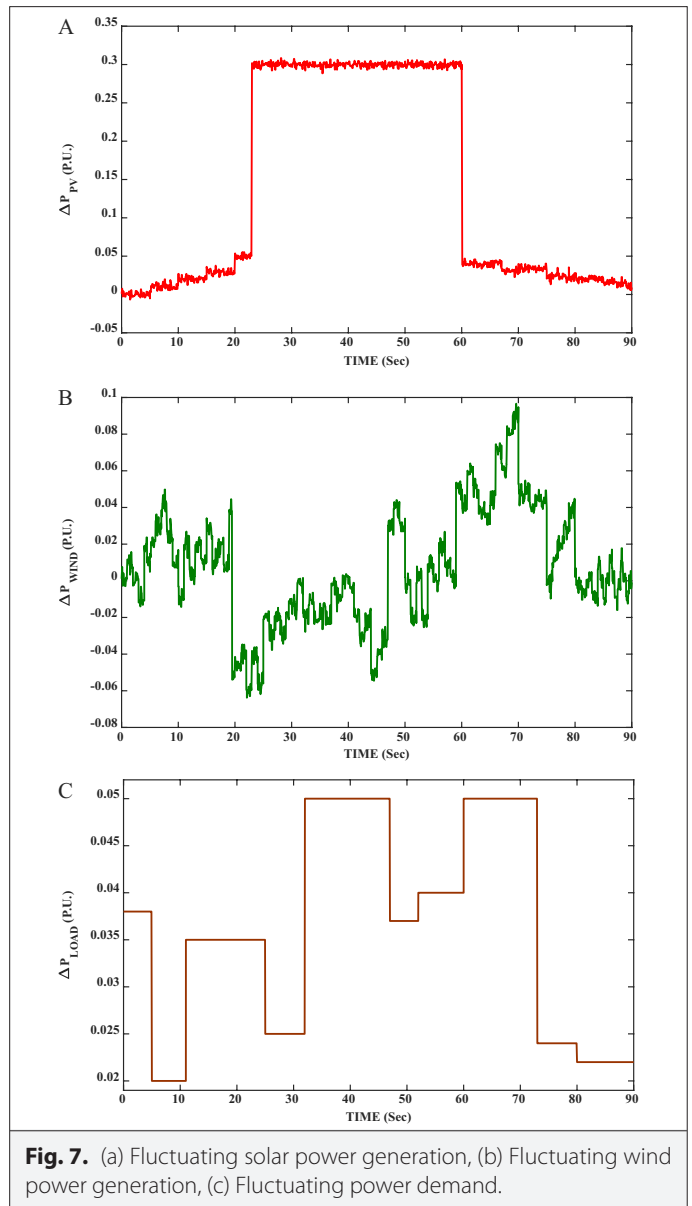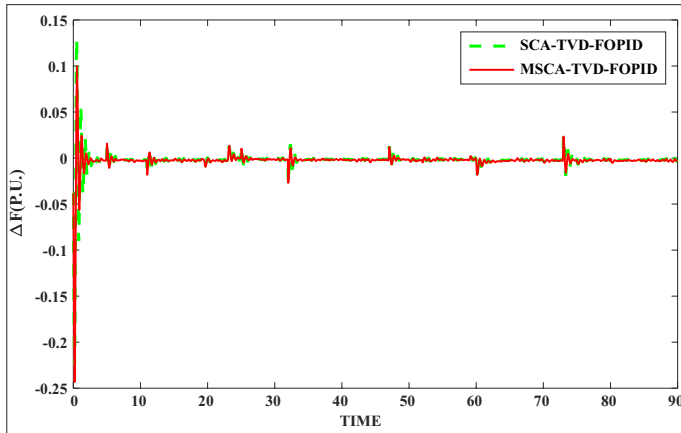
Fig. 9. Output frequency response for technique comparison.

Fig. 10. Output frequency response in sight of the power fluctuation.

TABLE II. GAIN PARAMETERS OBTAINED FROM SCA AND MSCA-TUNED TVD-FOPID CONTROLLER

Controller Parameters	MSCA	SCA
K_P	−1.909	1.1033
K_I	−2.987	−1.59
K_D	2.5	2.784
λ	0.0014	0.9077
M	0.0038	0.9038
α_1	−1.65	−1.385
ISE	0.038	0.044

ISE, integral square error; MSCA, modified sine cosine algorithm.

TABLE III. OPTIMAL GAIN VALUE OBTAINED FROM MSCA TUNED TVD-F OPID/TV-FOPID/FOPID CONTROLLERS

Controller Parameters	TVD-FOPID	TV-FOPID	FOPID
K_P	−1.909	2.909	−2.9
K_I	−2.987	−2.87	2.99
K_D	2.5	1.36	-2
λ	0.0014	0.9077	0.14
μ	0.0038	0.9038	0.0038
α_1	−1.65	−0.93	…
α_2	…	−2.987	…
α_3	…	−0.909	…

TABLE IV. TRANSIENT PERFORMANCE INDICES OBTAINED IN CASE 2

Performance Parameters	TVD-FOPID	TV-FOPID	FOPID
OS(+ve)	0.1294	1.0079	1.8184
US(-ve)	0.2252	0.3975	1.8052
TS(s)	0.0014	0.0025	1.3264
ISE	0.038	0.45	1.22
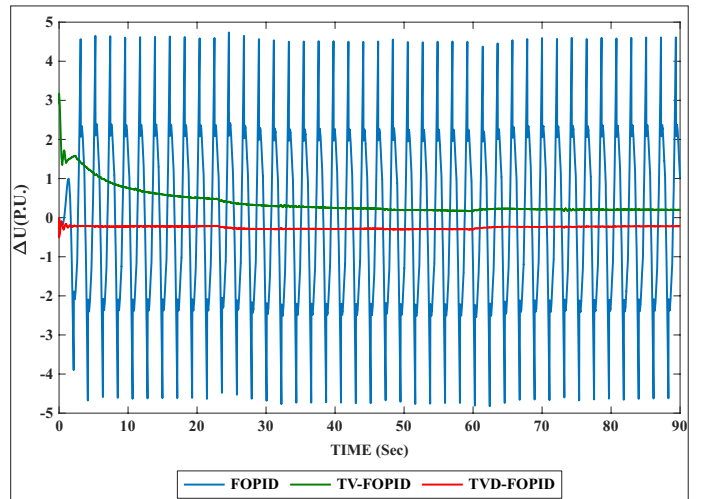
Fig. 11. Output voltage of controller's insight of power fluctuation.

well as lower voltage spikes in its output. Table VII entails the OS, US, TS, and fitness function values offered by the proposed TVD-FOPID controller compared with other considered TV-FOPID, and FOPID controllers. The proposed controller provides minimum values for all the transient parameters than that offered by other participant controllers.

E. Case 5: Validation in OPAL-RT
To study the real time compatibility of the proposed MSCA tuned TVD-FOPID controller for ship microgrid system, the MATLAB simulated model is executed in OPAL-RT 5700 simulator. The results obtained from the MATLAB simulator and OPAL-RT simulator are compared by using a software interface tool. The compared outcomes shown in Fig. 23, indicate the aliasing effect of both simulators, which justifies the practical feasibility of the proposed study.
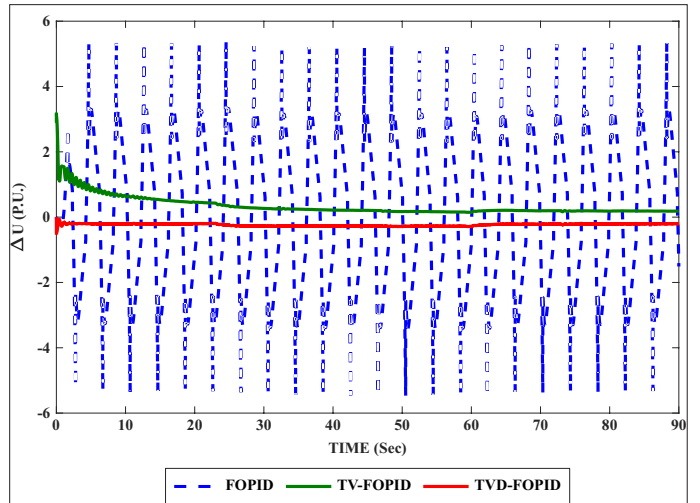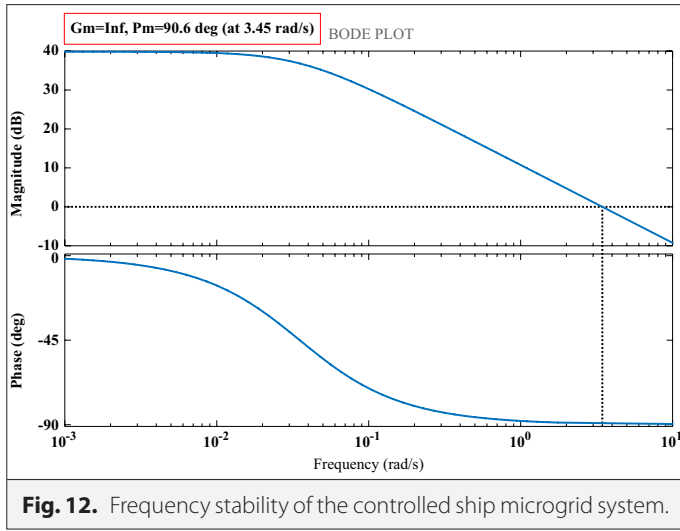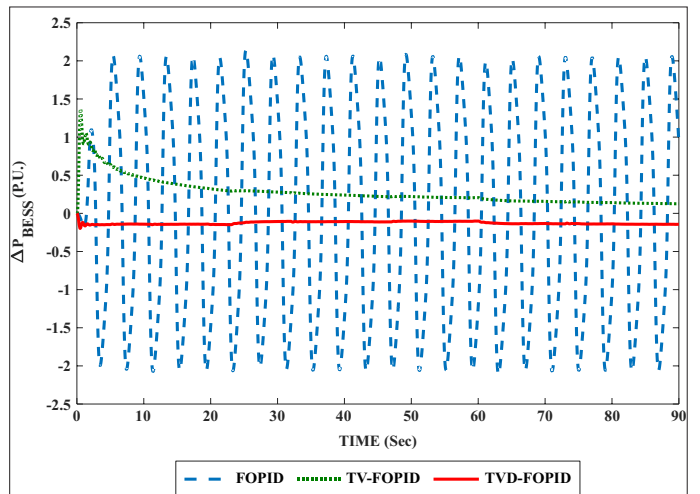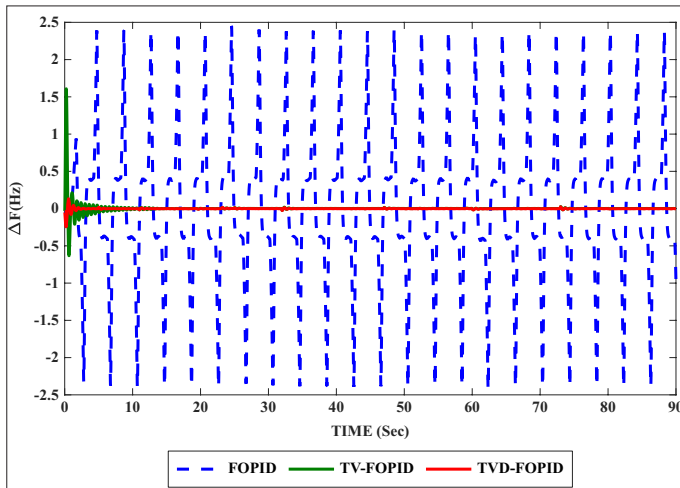
Fig. 12. Frequency stability of the controlled ship microgrid system.

TABLE V. CHANGED THE PARAMETERS OF SHIP MG

Parameters	Range of Variation
T_g	+15%
R	+25%
T_{FESS}	−15%
T_{BESS}	+25%
H	+45%
D	−15%

Fig. 13. Output frequency curve after varied ship parameters.

F. Case 6: Comparison With Recent Research Approaches

To evaluate the marginal gap established by the proposed MSCA: TVD-FOPID approach against some recently evolved frequency control approaches such as QOSCA: FOPI-D [21], SSA: 3DOF-TID and FOPID [19], GNA: FOPI-FOPTID [15], and h-WOA-SA: IT2F-FO-PID [17], a comparative analysis has been done. The dynamic condition of case 4 with random load, uncontrolled solar and wind power has

Fig. 14. Controller output voltage after varied ship parameters.

TABLE VI. TRANSIENT PROPERTIES OBTAINED IN CASE 3

Controller parameter	TVD-FOPID	TV-FOPID	FOPID
OS (+ve)	0.0137	1.6083	2.4456
US (−ve)	0.2451	0.6323	2.4262
TS (s)	0.0014	0.0014	1.9408
ISE	0.039	0.47	3.25

ISE, integral square error; OS, overshoot; TS, settling time; TV-FOPID, time-varying fractional order proportional–integral–derivative controller; TVD-FOPID, time-varying derivative fractional order proportional–integral–derivative controller; US, undershoot.

Fig. 15. Controlled power of BESS.

been considered for the comparison of frequency oscillations. The frequency fluctuation has been deployed in Fig. 24. From the deep analysis it is clear that the recent frequency control strategies are not able to provide sufficient damping at proper instant to slow down
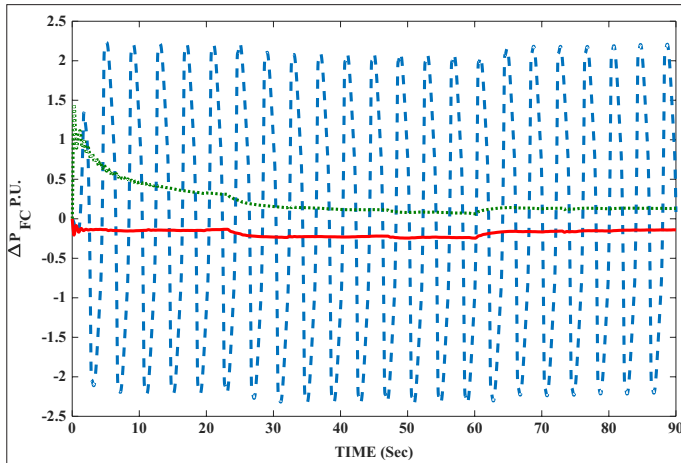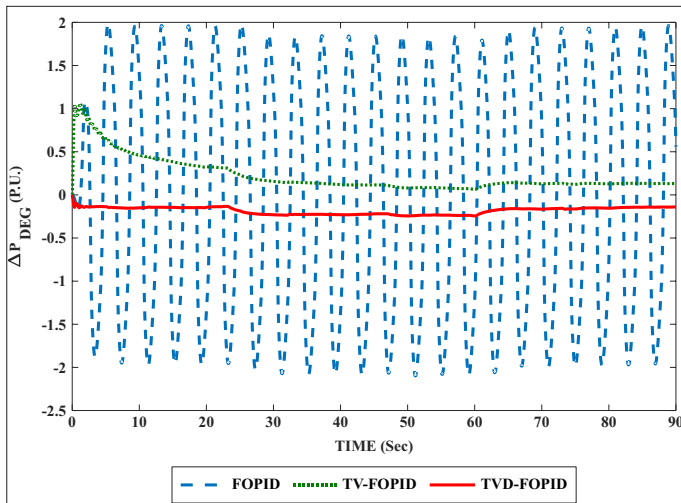
Fig. 16. Controlled power of FC
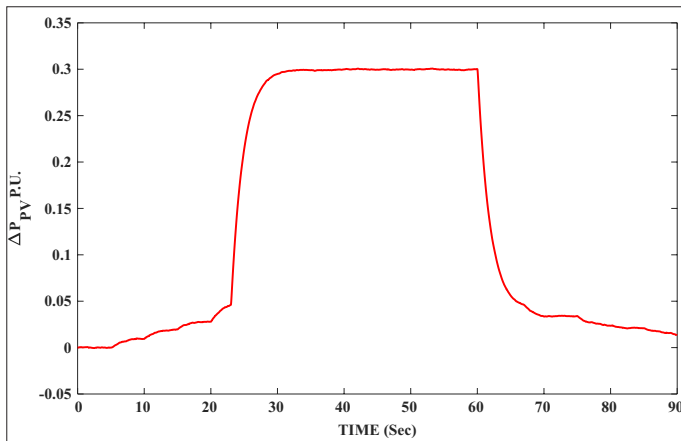

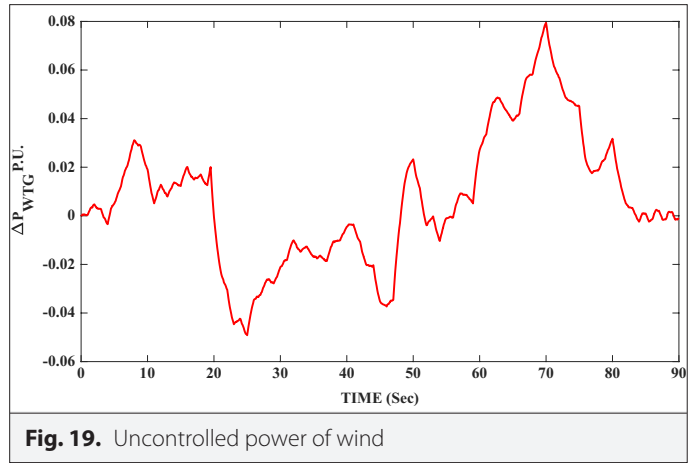**Fig. 17.** Controlled power of DEG

Fig. 18. Uncontrolled power of PV.

Fig. 19. Uncontrolled power of wind
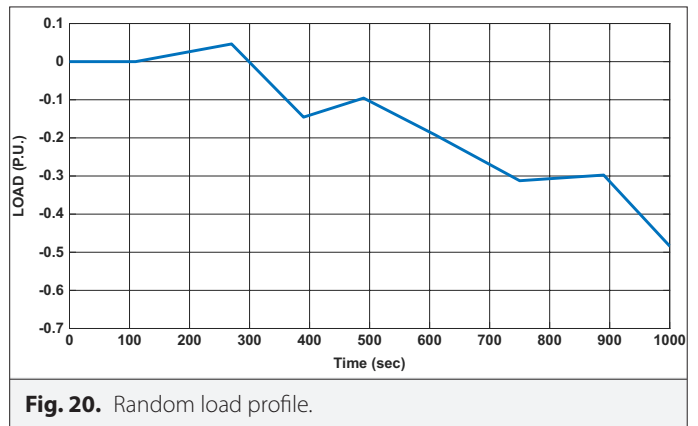
Fig. 20. Random load profile.
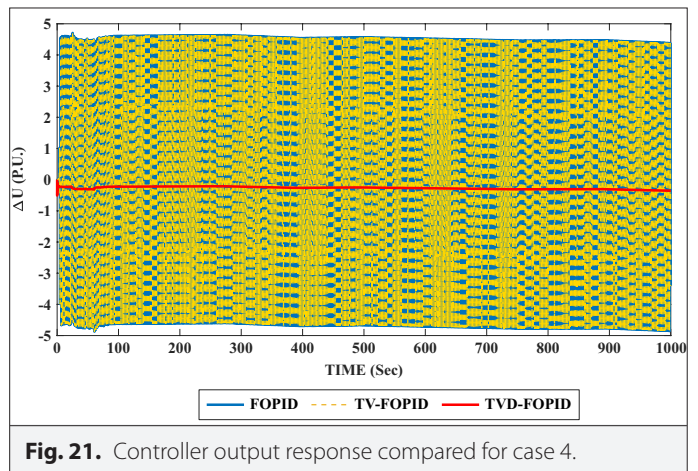
Fig. 21. Controller output response compared for case 4.

rapidly increasing transient period during critically disturbed situation of concern shipboard microgrid system. At the same intervals, the proposed MSCA scaled TVD-FOPID is offering optimal control action to restore the shipboard microgrid system frequency stability.

For high-dimensional complex system such as Shipboard MG system, computational complexity increases exponentially with the increment in dimension of the system. The performance of many popular optimizing tools is satisfactory for low-dimensional simple system, but they perform poorly when dealing with systems like Shipboard MG. From the observations, it was found that the basic MSA suffers from low solution accuracy due to poor global searching ability which makes slow premature local convergence as compared to MSCA. The MSCA offers better improved performance in resolving Shipboard MG system objective function with high-dimensional data set and unpredictable uncertainties. With the enhanced number
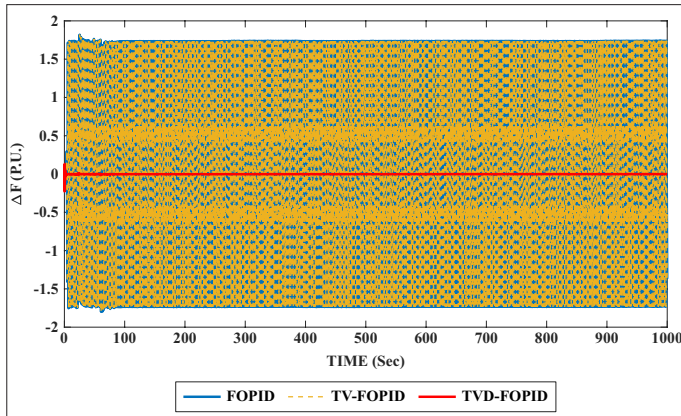
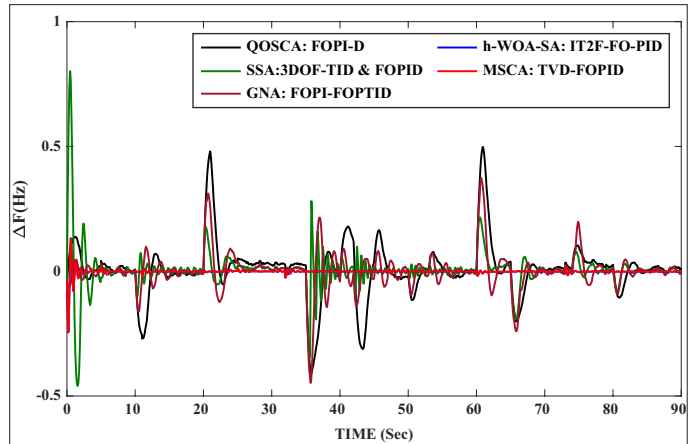**Fig. 22.** Frequency output response compared for case 4

Fig. 24. Frequency response compared for case 6

TABLE VII. TRANSIENT PROPERTIES OBTAINED IN CASE 4

Controller	TVD-FOPID	TV-FOPID	FOPID
OS (+ve)	1.3	1.8	1.8
US (−ve)	0.228	1.8	1.8
TS (s)	0.00093	0.601	0.606
ISE	0.1263	13.45	13.56

ISE, integral square error; OS, overshoot; TS, settling time; TV FOPID, time-varying fractional order proportional–integral–derivative controller; TVD FOPID, time-varying derivative fractional order proportional–integral–derivative controller; US, undershoot.
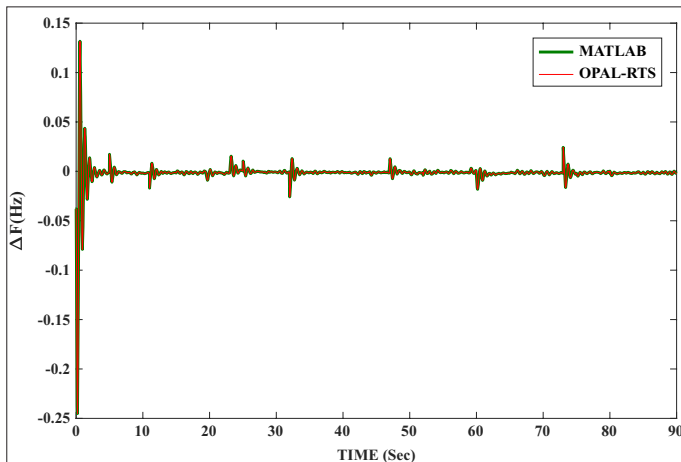

Fig. 23. Validation in OPAL-RT.

of iterations also the convergence was faster as compared to SCA and other techniques. The MSCA outperforms in terms all respects as compared to other methods. Hence, the above result analysis confirms the advantages of MSCA in resolving RESs integrated Shipboard nonlinear high-dimensional system's frequency regulation problem.

VI. CONCLUSION

In this research work, the recommended TVD-FOPID controller is designed for frequency control of the shipboard MG system. The

modified sine cosine algorithm (MSCA) is applied to tune the proposed TVD-FOPID controller parameters in the presence of fluctuating power of solar, wind power and load demand. It is noticed that, the ISE value is decreased by 13.63% with proposed MSCA-based TVD-FOPID controller compared to SCA -based TVD-FOPID controller. Similarly, the improvement in ISE value for MSCA-based TVD-FOPID is 91.6% in case 2, 91.7% in case 3, and 99% in case 4 as compared to MSCA-based TV-FOPID controller. It is also observed that in the presence of a TVD-FOPID controller, the voltage spike is reduced by about 40% and 99% as compared to TV-FOPID and regular FO-PID controllers. Also, the TVD-FOPID controller offers stable output in less time as compared to TV-FOPID and FOPID controllers. It is confirmed that the proposed controller is responsible for good damping of the system, as the derivative kick and the peak overshoot of the response offered by the proposed approach are decreased, which will save the life of the batteries and other control system apparatuses. For the varied range of parameters of the ship microgrid system, the controller has performed satisfactorily. This controller can be applied to any control system problem including hardware systems, which is suffering from severe derivative kick. In the future work, we will restructure the shipboard MG model including grid-forming inverters with other nonlinearities and improve the constraints of the proposed methods for optimal solution.

REFERENCES

1. H. Lan, Y. Bai, S. Wen, D. C. Yu, Y. Y. Hong, J. Dai and P. Cheng, "Modeling and Stability Analysis of Hybrid PV/Diesel/ESS in Ship Power System," *Inventions*, 1(1) (2016). [CrossRef]
2. Z. Jin, G. Sulligoi, R. Cuzner, L. Meng, J. C. Vasquez, and J. M. Guerrero, "Next-Generation Shipboard DC Power System: Introduction Smart Grid and dc microgrid Technologies into Maritime Electrical Networks," *IEEE Electrif. Mag.*, vol. 4, no. 2, pp. 45–57, 2016. [CrossRef]

3. E. Ovrum, and T. F. Bergh, "Modelling lithium-ion battery hybrid ship crane operation," *Appl. Energy*, vol. 152, pp. 162–172, 2015. [CrossRef]

4. B. Yildirim, M. Gheisarnejad, and M. H. Khooban, "Delay-dependent stability analysis of modern shipboard microgrids," *IEEE Trans. Circuits Syst. I*, vol. 68, no. 4, pp. 1693–1705, 2021. [CrossRef]

5. M. H. Khooban, T. Dragicevic, F. Blaabjerg, and M. Delimar, "Shipboard microgrids: A novel approach to load frequency control," *IEEE Trans. Sustain. Energy*, vol. 9, no. 2, pp. 843–852, 2017. [CrossRef]

6. M. Khamies, G. Magdy, M. E. Hussein, F. A. Banakhr, and S. Kamel, "An efficient control strategy for enhancing frequency stability of multi-area power system considering high wind energy penetration," *IEEE Access*, vol. 8, pp. 140062–140078, 2020. [CrossRef]

7. S. Mishra, S. Patel, R. C. Prusty, and S. Panda, "MVO optimized hybrid FOFPID-LQG controller for load frequency control of an AC micro-grid system," *World J. Eng.*, vol. 17, no. 5, pp. 675–686, 2020. [CrossRef]

8. E. Celik, N. Öztürk, and Y. Arya, "Advancement of the search process of salp swarm algorithm for global optimization problems," *Expert Syst. Appl.*, vol. 182, p. 115292, 2021. [CrossRef]

9. M. H. Khooban, T. Niknam, M. Shasadeghi, T. Dragicevic, and F. Blaabjerg, "Load frequency control in microgrids based on a stochastic noninteger controller," *IEEE Trans. Sustain. Energy*, vol. 9, no. 2, pp. 853–861, 2017. [CrossRef]

10. M. H. Khooban, and M. Gheisarnejad, "Islanded microgrid frequency regulations concerning the integration of tidal power units: Real-time implementation," *IEEE Trans. Circuits Syst. II*, vol. 67, no. 6, pp. 1099–1103, 2019. [CrossRef]

11. G. Sharma, N. Krishnan, Y. Arya, and A. Panwar, "Impact of ultracapacitor and redox flow battery with JAYA optimization for frequency stabilization in linked photovoltaic-thermal system," *Int. Trans. Electr. Energy Syst.*, vol. 31, no. 5, p. 12883, 2021. [CrossRef]

12. N. Hakimuddin, I. Nasiruddin, T. S. Bhatti, and Y. Arya, "Optimal automatic generation control with hydro, thermal, gas, and wind power plants in 2-area interconnected power system," *Electr. Power Compon. Syst.*, vol. 48, no. 6–7, pp. 558–571, 2020. [CrossRef]

13. P. Dahiya, P. Mukhija, and A. R. Saxena, "Event-triggered based decentralised control for frequency regulation of power systems," *IET Gener. Transm. Distrib.*, vol. 14, no. 10, pp. 2004–2015, 2020. [CrossRef]

14. P. Dahiya, P. Mukhija, and A. R. Saxena, "Design of sampled data and event-triggered load frequency controller for isolated hybrid power system," *Int. J. Electr. Power Energy Syst.*, vol. 100, pp. 331–349, 2018. [CrossRef]

15. R. Choudhary, J. N. Rai, and Y. Arya, "Cascade FOPI-FOPTID controller with energy storage devices for AGC performance advancement of electric power systems," *Sustain. Energy Technol. Assess.*, vol. 53, p. 102671, 2022. [CrossRef]

16. S. Oshnoei, A. Oshnoei, A. Mosallanejad, and F. Haghjoo, "Novel load frequency control scheme for an interconnected two-area power system including wind turbine generation and redox flow battery," *Int. J. Electr. Power Energy Syst.*, vol. 130, p. 107033, 2021. [CrossRef]

17. P. C. Nayak, S. Mishra, R. C. Prusty, and S. Panda, "Hybrid whale optimization algorithm with simulated annealing for load frequency controller design of hybrid power system," *Soft Comput.*, 2023. [CrossRef]

18. S. Oshnoei, A. Oshnoei, A. Mosallanejad, and F. Haghjoo, "Contribution of GCSC to regulate the frequency in multi-area power systems considering time delays: A new control outline based on fractional order controllers," *Int. J. Electr. Power Energy Syst.*, vol. 123, p. 106197, 2020. [CrossRef]

19. S. Oshnoei, M. Aghamohammadi, S. Oshnoei, A. Oshnoei, and B. Mohammadi-Ivatloo, "Provision of frequency stability of an islanded microgrid using a novel virtual inertia control and a fractional order cascade controller," *Energies*, vol. 14, no. 14, p. 4152, 2021. [CrossRef]

20. D. Mishra, P. C. Nayak, R. C. Prusty, and S. Panda, "An improved equilibrium optimization-based fuzzy tilted double integral derivative with filter (F-TIDF-2) controller for frequency regulation of an off-grid microgrid," *Electr. Eng.*, 2023. [CrossRef]

21. D. Guha, P. K. Roy, S. Banerjee, S. Padmanaban, F. Blaabjerg, and D. Chittathuru, "Small-signal stability analysis of hybrid power system with quasi-oppositional sine cosine algorithm optimized fractional order PID controller," *IEEE Access*, vol. 8, pp. 155971–155986, 2020. [CrossRef]

22. S. Mishra, R. C. Prusty, and S. Panda, "Performance analysis of modified sine cosine optimized multistage FOPD-PI controller for load frequency control of an islanded microgrid system," *Int. J. Numer. Modell. Electron. Netw. Devices Fields*, vol. 34, no. 6, 2021. [CrossRef]

23. L. Abualigah, and A. Diabat, "Advances in sine cosine algorithm: A comprehensive survey," *Artif. Intell. Rev.*, pp. 1–25, 2021. [CrossRef]

24. C. Qu, Z. Zeng, J. Dai, Z. Yi, and W. He, "A modified sine-cosine algorithm based on neighborhood search and greedy levy mutation," *Comp. Intell. Neurosci.*, vol. 2018, p. 4231647, 2018. [CrossRef]

25. S. Mirjalili, "SCA: A sine cosine algorithm for solving optimization problems," *Knowl. Based Syst.*, vol. 96, pp. 120–133, 2016. [CrossRef]

26. E. Yesil, "Interval type-2 fuzzy PID load frequency controller using Big Bang–Big Crunch optimization," *Appl. Soft Comput.*, vol. 15, pp. 100–112, 2014. [CrossRef]

27. A. Modirkhazeni, O. N. Almasi, and M. H. Khooban, "Improved frequency dynamic in isolated hybrid power system using an intelligent method," *Int. J. Electr. Power Energy Syst.*, vol. 78, pp. 225–238, 2016. [CrossRef]

28. D. Lee, and L. wang, "Small-signal stability analysis of an autonomous hybrid renewable power generation/energy storage system part1: Time-domain simulation," *IEEE Trans. Energy Convers.*, vol. 23, no. 1, pp. 311–320, 2008.

29. M. H. Khooban, T. Niknam, and M. Sha-Sadeghi, "Speed control of electrical vehicles: A time-varying proportional–integral controller-based type-2 fuzzy logic," *IET Sci. Meas. Technol.*, vol. 10, no. 3, pp. 185–192, 2016. [CrossRef]

30. S. Mishra, R. C. Prusty, and S. Panda, "Design and analysis of 2dof-PID controller for frequency regulation of multi-microgrid using hybrid dragonfly and pattern Search algorithm," *J. Control Autom. Electr. Syst.*, vol. 31, no. 3, pp. 813–827, 2020. [CrossRef]

31. K. Singh, M. Amir, F. Ahmad, and M. A. Khan, "An integral tilt derivative control strategy for frequency control in multi microgrid system," *IEEE Syst. J.*, vol. 15, no. 1, pp. 1477–1488, 2020. [CrossRef]

32. A. Lendek, and L. Tan, "Mitigation of derivative kick using time-varying fractional-order PID control," *IEEE Access*, vol. 9, pp. 55974–55987, 2021. [CrossRef]

33. N. Zhuo-Yun, Z. Yi-Min, W. Qing-Guo, L. Rui-Juan, and X. Lei-Jun, "Fractional-order PID controller design for time-delay systems based on modified Bode's ideal transfer function," *IEEE Access*, vol. 8, pp. 103500–103510, 2020. [CrossRef]

34. A. Mondal, A. Latif, D. C. Das, S. M. S. Hussain, and A. Al-Durra, "Frequency regulation of hybrid shipboard microgrid system using butterfly optimization algorithm synthesis fractional-order controller," *Int. J. Numer. Modell. Electron. Netw. Devices Fields*, vol. 36, no. 5, p. e3058, 2023. [CrossRef]

35. M. Bhuyan, D. C. Das, and A. K. Barik, "Chaotic butterfly optimization algorithm based cascaded PI-TID controller for frequency control in three area hybrid microgrid system," *Optimal Control Appl. Methods*, vol. 44, no. 5, pp. 2595–2619, 2023. [CrossRef]

36. E. Bahrampour, M. Dehghani, M. H. Asemani, and R. Abolpour, "Load frequency fractional-order controller design for shipboard microgrids using direct search algorithm," *IET Renew. Power Gener.*, vol. 17, no. 4, pp. 894–906, 2023. [CrossRef]

37. B. Yildirim, M. Gheisarnejad, and M. H. Khooban, "A robust non-integer controller design for load frequency control in modern marine power grids," *IEEE Trans. Emerg. Top. Comp. Intell.*, vol. 6, no. 4, pp. 852–866, 2022. [CrossRef]

Electrica 2024; 24(2): 392-405

Mishra et al. Design and Analysis of Time Varying Derivative Fractional Order PID Controller for Frequency Regulation of Shipboard Microgrid System

Dr Sonalika Mishra received the B.Tech. degree in Electrical and Electronics Engineering from the Biju Patnaik University of Technology, Odisha, India, 2014. She has received her M. Tech and PhD degree from Veer Surendra Sai University of Technology, Odisha, India. She is currently working as an Assistant Professor in the Electrical Engineering Department, Silicon Institute of Technology, Sambalpur, Odisha, India. Her current research interests include power system analysis, microgrids, power systems control, and renewable energy sources.

Dr Pratap Chandra Nayak received the B.Tech. and M. Tech degree in Electrical Engineering from the Biju Patnaik University of Technology, Odisha, India. He has received PhD degree from Veer Surendra Sai University of Technology, Odisha, India. He is currently working as an Assistant Professor in the Electrical Engineering Department at Biju Patnaik University of Technology. His current research interests include power system operation and control, microgrids, renewable energy sources and soft computing.

Dr Ramesh Chandra Prusty, Assistant Professor in the Electrical Engineering department, Veer Surendra Sai University of Technology, was born in India. He has received the B.Tech. degree from the Department of Electronics and Electrical Engineering, Biju Patnaik University of Technology, Odisha, the M.Tech. & PhD degree from the Department of Electrical Engineering, Veer Surendra Sai University of Technology, Burla, Odisha. His current research interests include artificial intelligence, power system & control system.

Dr. Sidhartha Panda, Professor in the Electrical Engineering Department, Veer Surendra Sai University of Technology, Burla, was born in India. He has received the M.Tech. degree from the Department of Electrical Engineering, Veer Surendra Sai University of Technology, Burla, Odisha & PhD degree from the Department of Electrical Engineering, IIT Roorkee. His current research interests include Soft computing, power system stability, automatic generation control, economic load dispatch & FACTS.